Analysis of Low-Momentum Correlations with Cartesian Harmonics

P. Danielewicz [a,b] and S. Pratt [b]

[a] *National Superconducting Cyclotron Laboratory and*

[b] *Department of Physics and Astronomy, Michigan State University, East Lansing, MI 48824-1321, USA*

Abstract

Exploiting final-state interactions and/or identity interference, analysis of anisotropic correlations of particles at low-relative velocities yield information on the anisotropy of emission sources in heavy-ion reactions. We show that the use of cartesian surface-spherical harmonics in such analysis allows for a systematic expansion of the correlations in terms of real angular-moment coefficients dependent on relative momentum. The coefficients are directly related to the analogous coefficients for emission sources. We illustrate the analysis with an example of correlations generated by classical Coulomb interaction.

Key words: correlation, interferometry, intensity interferometry, cartesian harmonics, anisotropic correlation
PACS: 25.70.Pq, 25.75.Gz

Correlations of particles at low relative velocities are commonly used for assessing geometric features of emission zones in nuclear reactions with multiparticle final states [1,2]. At low relative momentum, the correlations exhibit structures, due to final-state interactions and/or identity interference, that are more pronounced for tighter emission zones. When the shape of the emission zones is anisotropic, corresponding anisotropies are observed in the correlation function which can be studied as a function of the orientation of the relative momentum. Measured anisotropies in the correlation functions thus provide insight into the shape of the emission zone which is intimately connected to such aspects of the emission as reaction geometry, collective expansion, emission duration and differences in emission times for different species [3–5].

Final-state interactions and identity interference link the measured correlation function, $\mathcal{R}_{\mathbf{P}}(\mathbf{q})$ (or alternatively $\mathcal{C}_{\mathbf{P}}(\mathbf{q})$), to the source function, $\mathcal{S}_{\mathbf{P}}(\mathbf{r})$, which

provides the probability that two particles of the same velocity, whose total momentum is $\mathbf{P}$, are separated by a distance $\mathbf{r}$ at emission [6,7]:

$$\mathcal{R}_{\mathbf{P}}(\mathbf{q}) \equiv \mathcal{C}_{\mathbf{P}}(\mathbf{q}) - 1 \equiv \frac{\frac{\mathrm{d}^6 N^{ab}}{\mathrm{d}^3 p_a \, \mathrm{d}^3 p_b}}{\frac{\mathrm{d}N^a}{\mathrm{d}^3 p_a} \, \frac{\mathrm{d}N^b}{\mathrm{d}^3 p_b}} - 1 = \int \mathrm{d}^3 r \, \left[|\phi^{(-)}_{\mathbf{q}}(\mathbf{r})|^2 - 1 \right] \mathcal{S}^{ab}_{\mathbf{P}}(\mathbf{r}) \, . \quad (1)$$

Here, $\mathbf{q}$ and $\mathbf{r}$ are the relative momentum and relative spatial separation as determined by an observer in the two-particle rest frame and $\phi^{(-)}$ is the relative wave function for the asymptotic momentum $\mathbf{q}$. For particles with intrinsic spins, the square $|\phi^{(-)}|^2$ is averaged over spins.

Various means have been employed to analyze anisotropies in correlations and to provide quantitative measurement of the anisotropies in a source function. When analyzing identical pion correlations, the most common means has been to present projections of the correlation function along fixed directions of the relative momentum while constraining the remaining momentum components. Such projections often neglect regions of the data outside of the employed cuts and they are can be clumsy if one is unaware of the best directions to orient the coordinate system. A second means for analyzing anisotropies involves fitting to three-dimensional parameterizations, such as for gaussian or blast-wave models [8]. Since source parameterizations typically employ on the order of 10 parameters, it can be difficult to determine the confidence of the fits due to the inherent complexity of cross correlations.

A third class of approaches involves applying tesseral spherical harmonics, $Y_{\ell,m}$, to express the directional information in the correlation function and in the source function [9],

$$\begin{aligned} \mathcal{R}_{\ell m}(q) &= (4\pi)^{-1/2} \int \mathrm{d}\Omega_{\mathbf{q}} \, Y^*_{\ell m}(\Omega_{\mathbf{q}}) \, \mathcal{R}(\mathbf{q}) \, , \\ \mathcal{S}_{\ell m}(q) &= (4\pi)^{-1/2} \int \mathrm{d}\Omega_{\mathbf{r}} \, Y^*_{\ell m}(\Omega_{\mathbf{r}}) \, \mathcal{S}(\mathbf{r}). \end{aligned} \quad (2)$$

Here, the labels indicating the total momentum $\mathbf{P}$ and the particle types are suppressed. In terms of the projections, Eq. (1) can be re-expressed as

$$\mathcal{R}_{\ell m}(q) = 4\pi \int \mathrm{d}r \, r^2 \, K_\ell(q,r) \, \mathcal{S}_{\ell m}(r) \, , \quad (3)$$

where

$$K_\ell(q,r) = \frac{1}{2} \int \mathrm{d}\cos\theta_{\mathbf{qr}} \, P_\ell(\cos\theta_{\mathbf{qr}}) \, \left[|\phi(q,r,\cos\theta_{qr})|^2 - 1 \right] \, , \quad (4)$$

and $\theta_{\mathbf{qr}}$ is the angle between $\mathbf{q}$ and $\mathbf{r}$. Since a given ℓm projection of $\mathcal{R}$ is only

Table 1
Cartesian surface-spherical harmonics of rank $\ell \leq 4$. Other harmonics can be found by permuting indices or switching indices, i.e., $x \leftrightarrow y$, $x \leftrightarrow z$ or $y \leftrightarrow z$.

$\mathcal{A}^{(1)}_{x} = n_x$	$\mathcal{A}^{(3)}_{xyz} = n_x\, n_y\, n_z$
$\mathcal{A}^{(2)}_{xx} = n_x^2 - 1/3$	$A^{(4)}_{xxxx} = n_x^4 - (6/7)n_x^2 + 3/35$
$\mathcal{A}^{(2)}_{xy} = n_x\, n_y$	$\mathcal{A}^{(4)}_{xxxy} = n_x^3\, n_y - (3/7)n_x\, n_y$
$A^{(3)}_{xxx} = n_x^3 - (3/5)n_x$	$\mathcal{A}^{(4)}_{xxyy} = n_x^2\, n_y^2 - (1/7)n_x^2 - (1/7)n_y^2 + 1/35$
$\mathcal{A}^{(3)}_{xxy} = n_x^2\, n_y - (1/5)n_y$	$\mathcal{A}^{(4)}_{xxyz} = n_x^2\, n_y\, n_z - (1/7)n_y\, n_z$

related to the same ℓm projection of $\mathcal{S}$, the complexity of deconvoluting the shape information present in $\mathcal{R}$ is enormously simplified.

The disadvantage of projections with spherical harmonics is that the connection between the geometric features of the real source function $\mathcal{S}(\mathbf{r})$ and the complex valued projections $\mathcal{S}_{\ell m}(r)$ is not transparent. To rectify this shortcoming we propose performing a similar analysis with cartesian surface-spherical harmonics [10,11]. Cartesian harmonics are based on the products of unit vector components, $n_{\alpha_1}\, n_{\alpha_2} \cdots n_{\alpha_\ell}$. Due to the normalization identity $n_x^2 + n_y^2 + n_z^2 = 1$, at a given $\ell \geq 2$, the different component products are not linearly independent as functions of spherical angle; at a given ℓ, the products are spanned by tesseral harmonics of rank $\ell' \leq \ell$, with ℓ' of the same evenness as ℓ. Projecting away the lower-rank tesseral components, $\ell' < \ell$, is a linear operation in the ℓ-product space and produces cartesian rank-ℓ harmonics $\mathcal{A}^{(\ell)}_{\alpha_1 \cdots \alpha_\ell}(\Omega)$:

$$\mathcal{A}^{(\ell)}_{\alpha_1 \cdots \alpha_\ell} = \sum_{\alpha'_1 \ldots \alpha'_\ell} \mathcal{P}^{(\ell,\ell)}_{\alpha_1 \ldots \alpha_\ell, \alpha'_1 \ldots \alpha'_\ell}\, n_{\alpha'_1} \cdots n_{\alpha'_\ell}\,. \tag{5}$$

Tesseral harmonics of rank ℓ, are, in turn, expressible in terms of the powers of unit-vector components of the order $\ell' \leq \ell$, with ℓ' of the same evenness as ℓ. In the end, the harmonic $\mathcal{A}^{(\ell)}$ from (5) may be expressed as a combination of the powers of n_α of order $\ell' \leq \ell$, where ℓ' is of the same evenness as ℓ, as shown in Table 1. The leading term is a simple product of unit vectors with the same indices as $\mathcal{A}$. Since Cartesian harmonics $\mathcal{A}^{(\ell)}$ are lnear combinations of tesseral harmonics of order ℓ, the product $r^\ell\, \mathcal{A}^{(\ell)}$ satisfies the Laplace equation.

Because $\mathcal{A}^{(\ell)}$ is a linear combination of the tesseral harmonics of rank ℓ, and because the kernel in Eq. (3) depends only on ℓ (and not m), an analogous equation to (3) can be derived for cartesian harmonic coefficients:

$$\mathcal{R}^{(\ell)}_{\alpha_1 \cdots \alpha_\ell}(q) = 4\pi \int \mathrm{d}r\, r^2\, K_\ell(q,r)\, \mathcal{S}^{(\ell)}_{\alpha_1 \cdots \alpha_\ell}(r)\,, \tag{6}$$

where the coefficients are defined as

$$
\begin{aligned}
\mathcal{R}^{(\ell)}_{\alpha_1\ldots\alpha_\ell}(q) &= \frac{(2\ell+1)!!}{\ell!}\int\frac{\mathrm{d}\Omega_{\mathbf{q}}}{4\pi}\,\mathcal{A}^{(\ell)}_{\alpha_1\ldots\alpha_\ell}(\Omega_{\mathbf{q}})\,\mathcal{R}(\mathbf{q})\,,\\
\mathcal{S}^{(\ell)}_{\alpha_1\ldots\alpha_\ell}(q) &= \frac{(2\ell+1)!!}{\ell!}\int\frac{\mathrm{d}\Omega_{\mathbf{r}}}{4\pi}\,\mathcal{A}^{(\ell)}_{\alpha_1\ldots\alpha_\ell}(\Omega_{\mathbf{r}})\,\mathcal{S}(\mathbf{r})\,.
\end{aligned}
\tag{7}
$$

Cartesian harmonics satisfy the completeness relations:

$$
\begin{aligned}
\delta(\Omega'-\Omega) &= \frac{1}{4\pi}\sum_\ell\frac{(2\ell+1)!!}{\ell!}\sum_{\alpha_1\ldots\alpha_\ell}\mathcal{A}^{(\ell)}_{\alpha_1\ldots\alpha_\ell}(\Omega')\,\mathcal{A}^{(\ell)}_{\alpha_1\ldots\alpha_\ell}(\Omega)\\
&= \frac{1}{4\pi}\sum_\ell\frac{(2\ell+1)!!}{\ell!}\sum_{\alpha_1\ldots\alpha_\ell}\mathcal{A}^{(\ell)}_{\alpha_1\ldots\alpha_\ell}(\Omega')\,n_{\alpha_1}\cdots n_{\alpha_\ell}\,.
\end{aligned}
\tag{8}
$$

Replacing $\mathcal{A}^{(\ell)}(\Omega)$ with the product $n_{\alpha_1}\cdots n_{\alpha_\ell}$ was justified by the fact that the projection operator is employed in $\mathcal{A}^{(\ell)}(\Omega')$. Equation (8) allows one to restore $\mathcal{R}^{(\ell)}(q)$ and $\mathcal{S}^{(\ell)}(q)$ from the cartesian coefficients,

$$
\begin{aligned}
\mathcal{R}(\mathbf{q}) &= \sum_\ell\sum_{\alpha_1\ldots\alpha_\ell}\mathcal{R}^{(\ell)}_{\alpha_1\ldots\alpha_\ell}\,\hat{q}_{\alpha_1}\cdots\hat{q}_{\alpha_\ell}\,,\\
\mathcal{S}(\mathbf{r}) &= \sum_\ell\sum_{\alpha_1\ldots\alpha_\ell}\mathcal{S}^{(\ell)}_{\alpha_1\ldots\alpha_\ell}\,\hat{r}_{\alpha_1}\cdots\hat{r}_{\alpha_\ell}\,,
\end{aligned}
\tag{9}
$$

where $\hat{\mathbf{q}}$ and $\hat{\mathbf{r}}$ are unit vectors in the directions of $\mathbf{q}$ and $\mathbf{r}$.

Cartesian harmonics have other important properties. They are symmetric and traceless, i.e., if one sums $\mathcal{A}^{(\ell)}_{\alpha_1\cdots\alpha_\ell}$ over any two indices, the result is zero. In fact, the projection operator $\mathcal{P}$ in Eq. (5) is also referred to as a de-tracing operator. Tracelessness ensures, on its own, that $r^\ell\,\mathcal{A}^{(\ell)}$ satisfies the Laplace equation. While the z axis is singled out in the construction of tesseral harmonics, the axes are treated symmetrically in the construction of cartesian harmonics, and different components can be obtained from each other by interchanging the x, y and z axes. For instance, the expression for $\mathcal{A}^{(\ell=3)}_{yzz}$ can be found by replacing replacing n_x with n_z in the expression for $\mathcal{A}^{(\ell=3)}_{xxy}$ in Table 1. Cartesian harmonics can be also generated recursively, beginning with $\mathcal{A}^{(\ell=0)}=1$,

$$
\begin{aligned}
\mathcal{A}^{(\ell)}_{\alpha_1\ldots\alpha_\ell}(\Omega) &= \frac{1}{\ell}\sum_i n_{\alpha_i}\,\mathcal{A}^{(\ell-1)}_{\alpha_1\ldots\alpha_{i-1}\,\alpha_{i+1}\ldots\alpha_\ell}(\Omega) - \frac{2}{\ell(2\ell-1)}\\
&\quad\times\sum_{i<j}\sum_\alpha\delta_{\alpha_i\,\alpha_j}\,n_\alpha\,\mathcal{A}^{(\ell-1)}_{\alpha\,\alpha_1\ldots\alpha_{i-1}\,\alpha_{i+1}\ldots\alpha_{j-1}\,\alpha_{j+1}\ldots\alpha_\ell}(\Omega)\,.
\end{aligned}
\tag{10}
$$

The above recursion can be used to obtain the coefficients for expanding the cartesian harmonics in terms of unit vector components [11]. The strategy of recursion, carried out in the other direction, leads to the coefficients of expansion of the products in terms of harmonics:

$$n_x^{\ell_x}\, n_y^{\ell_y}\, n_z^{\ell_z} = \sum_{m_\alpha \le \ell_\alpha/2} \chi^{\ell_x,\ell_y,\ell_z}_{m_x,m_y,m_z}\, \mathcal{A}^{(\ell-2m)}_{[\ell_x-2m_x,\ell_y-2m_y,\ell_z-2m_z]}\,, \tag{11}$$
$$\chi^{\ell_x,\ell_y,\ell_z}_{m_x,m_y,m_z} \equiv \frac{(2\ell-4m+1)!!}{2^m\,(2\ell-2m+1)!!} \prod_{\alpha=x,y,z} \frac{\ell_\alpha!}{m_\alpha!\,(\ell_\alpha-2m_\alpha)!}\,.$$

Here, $(-1)!! = 1$, $m = m_x + m_y + m_z$, $\ell = \ell_x + \ell_y + \ell_z$ and $[\ell_x, \ell_y, \ell_z]$ is any set of indices where x occurs ℓ_x times, y occurs ℓ_y times and z occurs ℓ_z times. This expansion is useful for calculating moments of $\mathcal{S}(\mathbf{r})$,

$$\int \mathrm{d}^3r\, x^{\ell_x}\, y^{\ell_y}\, z^{\ell_z}\, \mathcal{S}(\mathbf{r}) \Big/ \int \mathrm{d}^3r\, \mathcal{S}(\mathbf{r}) = \sum_{m_\alpha \le \ell_\alpha/2} \frac{(\ell-2m)!}{(2\ell-4m+1)!!}\, \chi^{\ell_x,\ell_y,\ell_z}_{m_x,m_y,m_z}$$
$$\cdot \int \mathrm{d}r\, r^{\ell+2}\, \mathcal{S}^{(\ell-2m)}_{[\ell_x-2m_x,\ell_y-2m_y,\ell_z-2m_z]}(r) \Big/ \int \mathrm{d}r\, r^2\, \mathcal{S}^{(0)}(r)\ . \tag{12}$$

Since rank-ℓ cartesian harmonics are linear combinations of rank-ℓ tesseral harmonics, cartesian harmonics of different ℓ are orthogonal to one another. Within a given rank, though, there are $(\ell+1)(\ell+2)/2$ combinations of $[\ell_x, \ell_y, \ell_z]$, while only $(2\ell+1)$ components can be independent. As an independent set, one can choose the components characterized by $\ell_\alpha = 0, 1$, for a selected coordinate α, and the remaining harmonics within the rank can be generated via the traceleness property. For example, given harmonics for $\ell_x = 0, 1$, $\mathcal{A}_{[\ell_x+2,\ell_y,\ell_z]} = -\mathcal{A}_{[\ell_x,\ell_y+2,\ell_z]} - \mathcal{A}_{[\ell_x,\ell_y,\ell_z+2]}$ provides the other harmonics. As for scalar product values within a rank, they can be found in [11].

For weak physical anisotropies it is likely that only few lowest terms of angular expansion can be ascribed to the correlation functions or the source. For $\ell \le 2$, the results can be summarized in terms of amplitudes and direction vectors as a function of q and r, as illustrated here with the case of $\mathcal{R}$:

$$\mathcal{R}(\mathbf{q}) = \mathcal{R}^{(0)}(q) + \sum_\alpha \mathcal{R}^{(1)}_\alpha(q)\, \hat{q}_\alpha + \sum_{\alpha_1\,\alpha_2} \mathcal{R}^{(2)}_{\alpha_1\alpha_2}(q)\, \hat{q}_{\alpha_1}\, \hat{q}_{\alpha_2} + \dots\,. \tag{13}$$

The function $\mathcal{R}^{(0)}$ is the correlation averaged over angles. The $\mathcal{R}^{(1)}$ components describe the dipole anisotropy and can be summarized in terms of the direction $\mathbf{e}^{(1)}(q)$ and magnitude $R^{(1)}(q)$, $\mathcal{R}^{(1)}_\alpha(q) = R^{(1)}\, e^{(1)}_\alpha$. The $\mathcal{R}^{(2)}$ components describe the quadrupole anisotropy and can be summarized in terms of three orthogonal principal direction vectors $\{\mathbf{e}^{(2)}_k(q)\}_{k=1,2,3}$ and three distortions that sum up to zero due to tracelessness: $\mathcal{R}^{(2)}_{\alpha\beta}(q) = R^{(2)}_1\, e^{(2)}_{1\alpha}\, e^{(2)}_{1\beta} + R^{(2)}_3\, e^{(2)}_{3\alpha}\, e^{(2)}_{3\beta} - \left(R^{(2)}_1 + R^{(2)}_3\right) e^{(2)}_{2\alpha}\, e^{(2)}_{2\beta}$. For higher-order distortions, the direction of maximal distortion $\mathbf{e}^{(\ell)}_3$ may be defined as one maximizing the ℓ'th cartesian harmonic projected in the direction of $\mathbf{e}_3$: $\sum_{\alpha_1\dots\alpha_\ell} \mathcal{R}^{(\ell)}_{\alpha_1\dots\alpha_\ell}\, \mathbf{e}^{(\ell)}_{3\alpha_1} \cdots \mathbf{e}^{(\ell)}_{3\alpha_\ell}$. The condition of maximum implies $\sum_{\alpha_1\dots\alpha_\ell} \mathcal{R}^{(\ell)}_{\alpha_1\,\alpha_2\dots\alpha_\ell}\, e^{(\ell)}_{k\,\alpha_1}\, e^{(\ell)}_{3\,\alpha_2} \cdots e^{(\ell)}_{3\,\alpha_n} = 0$, where

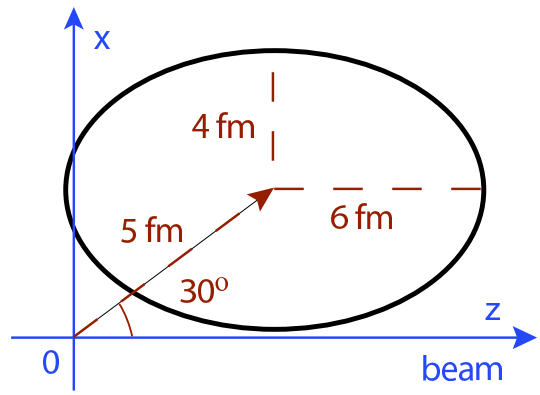

Fig. 1. Characteristics of the sample source. The ellipse represents the contour of constant density within x-z plane, at half the maximum density.

$k = 1, 2$ and $\mathbf{e}_1^{(\ell)}$ and $\mathbf{e}_2^{(\ell)}$ span the space of directions perpendicular to $\mathbf{e}_3^{(\ell)}$. The direction of $\mathbf{e}_1^{(\ell)}$ may be chosen to minimize the projection of $\mathcal{C}^{(\ell)}$ in the plane perpendicular to $\mathbf{e}_3^{(\ell)}$.

We next illustrate with an example how the correlation functions and source can be quantified following the cartesian coefficients. We choose a coordinate system with the z-axis along the beam direction and x-axis along the pair transverse momentum $\mathbf{P}^{\perp}$. We take a sample relative source for the particles, in a gaussian form with a larger 6 fm width in the beam direction and lower 4 fm widths in the transverse directions, cf. Fig. 1. The source is displaced from the origin by 5 fm, along $\mathbf{P}$ in system cm, assumed to point at 30° relative to the beam axis. Representations of the source in cartesian harmonics are then calculated numerically according to Eq. (6). The dipole distortion is then expressed as a magnitude and an angle, $S^{(1)} \sin\theta_S^{(1)} = \mathcal{S}_x^1 = 3\int \frac{\mathrm{d}\Omega}{4\pi}\mathcal{S}(\mathbf{r})\sin\theta$ and $S^{(1)}\cos\theta_S^{(1)} = \mathcal{S}_z^{(1)} = 3\int\frac{\mathrm{d}\Omega}{4\pi}\mathcal{S}(\mathbf{r})\cos\theta$. The quadrupole distortions are represented in terms of two distortions and an angle: $\mathcal{S}_{xx}^{(2)} = S_1^{(2)}\cos^2\theta_S^{(2)} + S_3^{(2)}\sin^2\theta_S^{(2)}$, $\mathcal{S}_{zz}^{(2)} = S_1^{(2)}\sin^2\theta_S^{(2)} + S_3^{(2)}\cos^2\theta_S^{(2)}$ and $\mathcal{S}_{xz}^{(2)} = \left(S_3^{(2)} - S_1^{(2)}\right)\sin^2\theta_S^{(2)}$, where $\mathcal{S}_{xx}^{(2)} = \frac{15}{2}\int\frac{\mathrm{d}\Omega}{4\pi}\mathcal{S}(\mathbf{r})\left(\sin^2\theta\cos^2\phi - \frac{1}{3}\right)$, $\mathcal{S}_{zz}^{(2)} = \frac{15}{2}\int\frac{\mathrm{d}\Omega}{4\pi}\mathcal{S}(\mathbf{r})\left(\cos^2\theta - \frac{1}{3}\right)$ and $\mathcal{S}_{xz}^{(2)} = \frac{15}{2}\int\frac{\mathrm{d}\Omega}{4\pi}\mathcal{S}(\mathbf{r})\cos\theta\sin\theta\cos\phi$.

Figure 2 displays the cartesian representations of the source, $S^{(0)}(r)$, $S^{(1)}(r)$, $S_3^{(2)}(r)$ and $S_1^{(2)}(r)$, Despite the fact that the maximum source density occurs away from $\mathbf{r} = 0$, the angle-averaged source, $\mathcal{S}^{(0)}$ is a maximum at $r = 0$. Since the source function is analytic, it can be expanded about $\mathbf{r} = 0$ in a three-dimensional Taylor expansion. The lowest order term in the Taylor expansion that can contribute to an ℓth-order cartesian harmonics must involve ℓ derivatives and rise as r^ℓ as can be seen with $S^{(1)}$ and $S^{(2)}$ functions in Fig. refsourcemo. This property, that $\mathcal{S}^{(\ell)}$ expands as $r^\ell, r^{\ell+2}, \cdots$, is important if one tries to parameterize the source functions.

Figure 3 shows the angles, $\theta^{(1)}$ and $\theta^{(2)}$ characterizing dipole and quadrupole

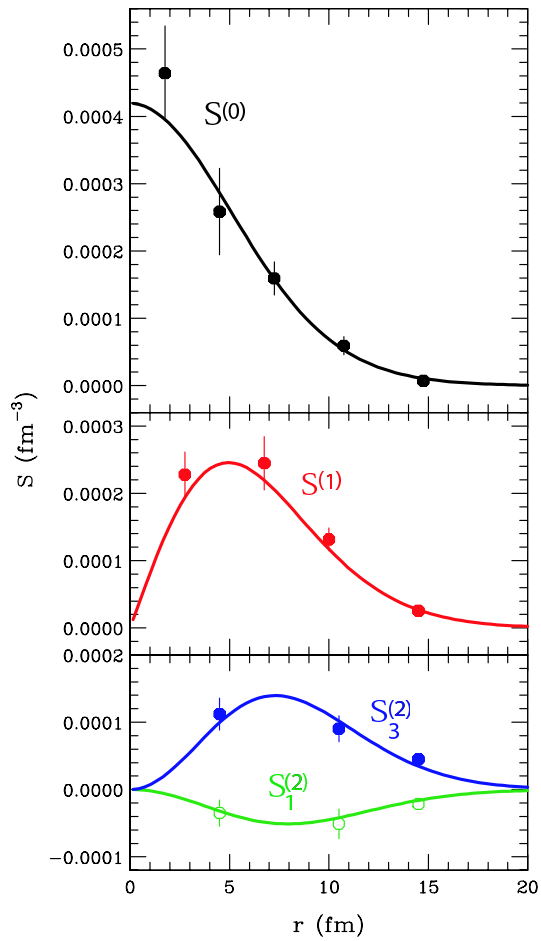

Fig. 2. Low-ℓ values of the sample relative source, as a function of the relative distance r. Lines and symbols represent, respectively, exact values and values obtained through imaging of an anisotropic correlation function. Top panel shows the source averaged over angles, $S^{(0)}$. Middle panel shows the dipole distortion $S^{(1)}$. Bottom panel shows the larger, $S_3^{(2)}$, and smaller, $S_1^{(2)}$, quadrupole distortions within the x-z plane.

distortions of the sample source. At low r both angles are affected by both the distortions in center of the source and by the fact that $R_z \neq R_x$, and $\theta^{(1)}$ starts out at 52° while $\theta^{(2)}$ starts out at 28°. At high r, the direction is dominated by the anisotropy of the Gaussian, and both angle approach zero as $r \to \infty$.

Next, we determine correlation function coefficients for our sample source, examine how the coefficients reflect the source features and attempt to restore those features through imaging. We choose the classical limit of Coulomb interactions for the emitted particles, such as appropriate for intermediate mass fragments [12,13]. The kernel for Eqs. (1) and (4) can be analytically calculated from the focusing/de-focusing of Coulomb trajectories, $\phi^2 \sim d^3q_0/d^3q$, where q_0 is the original momentum. Then result depends only on the angle $\theta_{\mathbf{qr}}$ and on the separation at emission scaled with the distance of closest approach

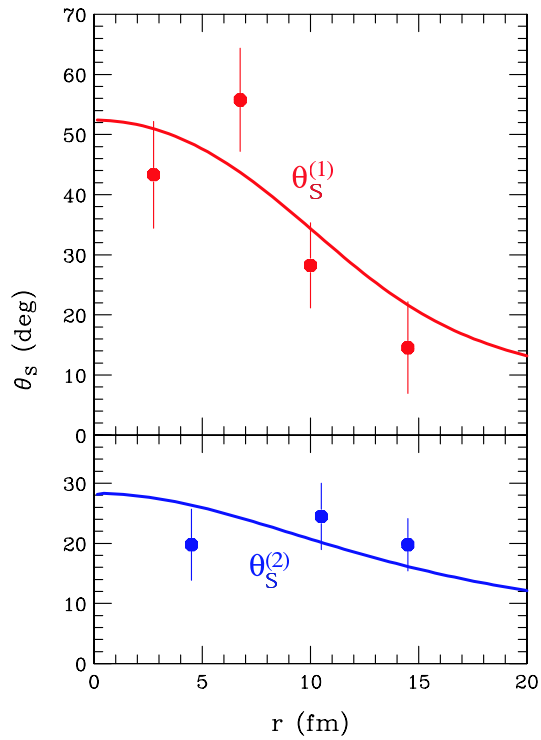

Fig. 3. Angles characterizing the dipole (top) and quadrupole (bottom) distortions of the sample relative source, as a function of the relative distance r. Lines and symbols represent, respectively, exact angles and angles obtained from imaging of an anisotropic correlation function.

in a head-on collision, r/r_c, where $q^2/2m_{ab} = Z_a\, Z_b\, e^2/4\pi\epsilon_0\, r_c$:

$$|\phi(q, r, \cos\theta_{qr})|^2 = \frac{\Theta\,(1+\cos\theta_{\mathbf{qr}} - 2r_c/r)\,(1+\cos\theta_{\mathbf{qr}} - r_c/r)}{\sqrt{(1+\cos\theta_{\mathbf{qr}})^2 - (1+\cos\theta_{\mathbf{qr}})\,2r_c/r}}\,. \tag{14}$$

The $\ell = 0$ kernel is $K_0 = \Theta(r - r_c)\,\sqrt{1 - r_c/r} - 1$, while the $K_{\ell\geq 1}$ components are calculated numerically from (4).

The Coulomb trajectories are illustrated in Fig. 4. If the source points are biased in a given direction, the repulsive Coulomb force focuses the trajectories in the same direction. For large r/r_c (either large r or large q) the kernels are affected by the deflection of the trajectories which with $\cos\theta_{qr} \sim -1$. Since $P_\ell(\cos\theta \to -1) = (-1)^\ell$, the sign of the kernel behaves as $(-1)^\ell$. Thus, the dipole representation of $\mathcal{S}^{(1)}$ points away from the direction of the shadowing, i.e., towards the angle where the particles predominantly originate. The projection of the quadrupole moment in this direction has the opposite sign. As r/r_c falls (r or q becomes smaller), the $\ell > 1$ kernels will switch signs $\ell - 1$ times. For $\ell = 2$, this switch occurs at $r/r_c = 1.63$. This means that for $r/r_c > 1.63$, a prolate source gives an oblate distortion to the correlation, while for $r/r_c < 1.63$, a prolate source results in a prolate distortion to the

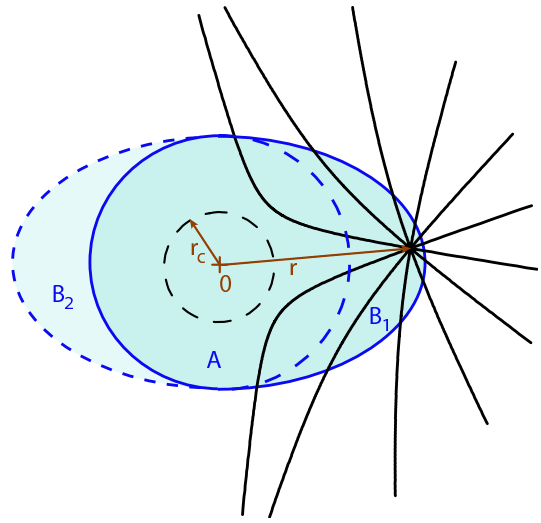

Fig. 4. A schematic relative source with repulsive Coulomb trajectories superimposed coming out isotropically from position $\mathbf{r}$ within the source. The region of radius r_c is inaccessible for the trajectories. The source consists of an isotropic part A, axially symmetric part B_1, responsible for source deformation, and, optionally, part B_2 that is a mirror reflection of B_1.

correlation.

Figure 5 shows the characteristics of the correlation function $\mathcal{C}$, in terms of $\ell \leq 2$ cartesian coefficients, for the source of Fig. 1, as function of $r_c^{-1/2} \propto q$. The dependence $\theta_C^{(1)}(r_c)$ in Fig. 5 generally retraces the dependence $\theta_S^{(1)}(r)$ of Fig. 3, where $r_c \lesssim r$. This can be understood in terms of Coulomb trajectories in Fig. 4 that get always deflected away from origin, for any r/r_c. The situation is more complicated with $\theta_C^{(2)}$. Since the kernel behaves as $(-1)^\ell$ for large r/r_c, the prolate source produces an oblate distortion to the correlation which means the $\theta^{(2)}$ points to a direction which is 90 degrees off the direction to which the source density is biased. At low r_c, the kernel switches sign and $\theta^{(2)}$ again aligns with the direction to which the source is biased.

We next illustrate imaging of source components from the correlation [9,14–18]. The tensorial decomposition allows to use different source representations within subspaces of different tensorial rank. With a source coefficient represented in the basis $\{B_i\}$ as $\mathcal{S}(r) = \sum_i \mathcal{S}_i\, B_i(r)$, the $\mathcal{R}$ function at j'th discrete value of q (or $r_c^{-1/2}$ in our case), is $\mathcal{R}_j = K_{ji}\, \mathcal{S}_i$, where $K_{ji} = 4\pi \int_0^\infty \mathrm{d}r\, r^2\, K(q_j, r)\, B_i(r)$. Minimization of $\chi^2 = \sum_j (\mathcal{R}_j - \mathcal{R}_j^{exp})^2/\sigma_j^2$ with respect to $\{S_i\}$ yields the result, in matrix form,

$$\mathcal{S} = (K^\top\, \sigma_{\mathcal{C}}^{-2}\, K)^{-1}\, K^\top\, \sigma_{\mathcal{C}}^{-2}\, \mathcal{R}\,, \tag{15}$$

where $(\sigma_{\mathcal{C}}^{-2})_{jk} = \delta_{jk}/\sigma_j^2$. For illustration, we assume that the $\ell \leq 2$ cartesian coefficients of the correlation function for our sample source have been mea-

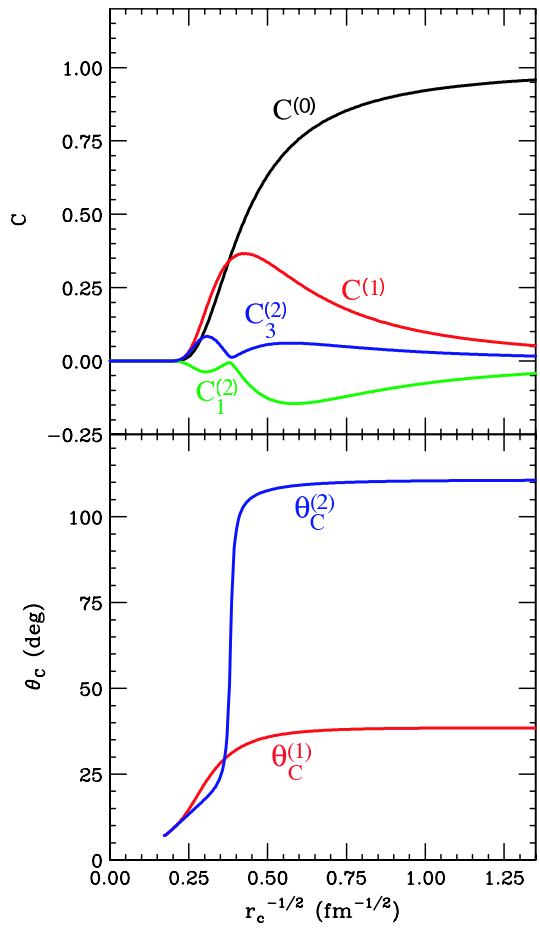

Fig. 5. Low-ℓ characteristics of the Coulomb correlation function for our sample source: amplitudes (top panel) and angles (bottom panel) as a function of inverse square root of the head-on return radius r_c.

sured at 80 values of $r_c^{-1/2}$, between 0 and $3\,\mathrm{fm}^{-1/2}$, subject to an r.m.s. error of $\sigma = 0.015$. For $\{B_i\}$ we take take simple rectangle functions that, within basis splines, we find to provide the most faithful source values. As relative errors decrease with increasing multipolarity, we reduce the number of functions in restoration, from 5 for $\ell = 0$ to 3 for $\ell = 2$, all spanning the region $r < 17\,\mathrm{fm}$. Upon sampling the cartesian coefficients of $\mathcal{R}$, we restore the coefficients of $\mathcal{S}$ following (15) and obtain the results represented by symbols in Figs. 2 and 3 for central arguments of the basis functions. As is apparent, under realistic circumstances, angular features of the source can be quantitatively restored.

Having the imaged $\ell \leq 2$ source coefficients, we can calculate the $\ell \leq 2$ cartesian moments for the imaged region from (12). For the image we find, with statistical errors of restoration: $4\pi \int \mathrm{d}r\, r^2\, \mathcal{S}^{(0)} = 0.99 \pm 0.05$, $\langle x \rangle = (1/3) \int \mathrm{d}r\, r^3\, \mathcal{S}_x^{(1)} / \int \mathrm{d}r\, r^2\, \mathcal{S}^{(0)} = 2.47 \pm 0.11\,\mathrm{fm}$, $\langle z \rangle = 4.25 \pm 0.13\,\mathrm{fm}$, $\langle (x - \langle x \rangle)^2 \rangle^{1/2} = 3.80 \pm 0.24\,\mathrm{fm}$, $\langle y^2 \rangle^{1/2} = 3.81 \pm 0.22\,\mathrm{fm}$, $\langle (z - \langle z \rangle)^2 \rangle^{1/2} = 5.54 \pm 0.19\,\mathrm{fm}$ and $\langle (x - \langle x \rangle)(z - \langle z \rangle) \rangle = 2.23 \pm 1.49\,\mathrm{fm}^2$, which can be compared to the $r < 17\,\mathrm{fm}$ results from the original source of, respectively: 1.00,

2.45 fm, 3.90 fm, 3.99 fm, 4.00 fm, 5.60 fm and $-0.41\,\mathrm{fm}^2$.

In summary, we have discussed the utility of cartesian surface-spherical harmonics in the analysis of particle correlations at low relative-velocities. The cartesian harmonics allow for a systematic quantification of anisotropic correlation functions, through expansion coefficients related to analogous expansion coefficients for anisotropic emission sources. For illustrating the relation, we have employed correlations produced by classical Coulomb interactions. To an extent, the features of source anisotropies may be read off directly from the correlation anisotropies; otherwise, they can be imaged.

Acknowledgements

The authors thank David Brown for discussions and for collaboration on a related project. This work was supported by the U.S. National Science Foundation under Grant PHY-0245009 and by the U.S. Department of Energy under Grant No. DE-FG02-03ER41259.

References

[1] U. W. Heinz and B. V. Jacak, Ann. Rev. Nucl. Part. Sci. **49** (1999) 529.

[2] W. Bauer, C. K. Gelbke and S. Pratt, Ann. Rev. Nucl. Part. Sci. **42** (1992) 77.

[3] R. Lednicky, V. L. B. Erazmus and D. Nouais, Phys. Lett. B **373** (1996) 20.

[4] S. Voloshin, R. Lednicky and S. Panitkin, Phys. Rev. Lett. **79** (1997) 4766.

[5] C. J. Gelderloos *et al.*, Phys. Rev. Lett. **75** (1995) 3082.

[6] S. E. Koonin, Phys. Lett. B **70** (1977) 43.

[7] D. Anchishkin, U. W. Heinz and P. Renk, Phys. Rev. C **57** (1998) 1428.

[8] F. Retiere and M. A. Lisa, Phys. Rev. C **70** (2004) 044907.

[9] D. A. Brown and P. Danielewicz, Phys. Lett. B **398** (1997) 252.

[10] J. Applequist, J. Phys. A: Math. Gen. **22** (1989) 4303.

[11] J. Applequist, Theor. Chem. Acc. **107** (2002) 103.

[12] Y. Kim, R. de Souza, C. Gelbke, W. Gong, and S. Pratt, Phys. Rev. C **45** (1992) 387.

[13] S. Pratt and S. Petriconi, Phys. Rev. C **68** (2003) 054901.

[14] D. A. Brown and P. Danielewicz, Phys. Rev. C **64** (2001) 014902.

[15] S. Y. Panitkin *et al.*, Phys. Rev. Lett. **87** (2001) 112304.

[16] G. Verde *et al.*, Phys. Rev. C **65** (2002) 054609.

[17] G. Verde *et al.*, Phys. Rev. C **67** (2003) 034606.

[18] P. Chung *et al.*, Phys. Rev. Lett. **91** (2003) 162301.